High Power Laser Science and Engineering, (2024), Vol. 12, e66, 9 pages.
doi:10.1017/hpl.2024.42

HIGH POWER LASER SCIENCE AND ENGINEERING

RESEARCH ARTICLE

Diode-pumped high-power gigahertz Kerr-lens mode-locked solid-state oscillator enabled by a dual-confocal ring cavity

Li Zheng[1,2], Wenlong Tian[1], Hanchen Xue[3], Yuehang Chen[1], Geyang Wang[1], Chuan Bai[1], Yang Yu[4], Zhiyi Wei[3], and Jiangfeng Zhu[1]

[1] *School of Optoelectronic Engineering, Xidian University, Xi'an, China*

[2] *School of Physics and Telecommunication Engineering, Shaanxi University of Technology, Hanzhong, China*

[3] *Beijing National Laboratory for Condensed Matter Physics and Institute of Physics, Chinese Academy of Sciences, Beijing, China*

[4] *Academy of Advanced Interdisciplinary Research, Xidian University, Xi'an, China*

(Received 12 April 2024; revised 4 June 2024; accepted 9 July 2024)

Abstract

Femtosecond oscillators with gigahertz (GHz) repetition rate are appealing sources for spectroscopic applications benefiting from the individually accessible and high-power comb line. The mode mismatch between the potent pump laser diode (LD) and the incredibly small laser cavity, however, limits the average output power of existing GHz Kerr-lens mode-locked (KLM) oscillators to tens of milliwatts. Here, we present a novel method that solves the difficulty and permits high average power LD-pumped KLM oscillators at GHz repetition rate. We propose a numerical simulation method to guide the realization of Kerr-lens mode-locking and comprehend the dynamics of the Kerr-lens mode-locking process. As a proof-of-principle demonstration, an LD-pumped Yb:KGW oscillator with up to 6.17-W average power and 184-fs pulse duration at 1.6-GHz repetition rate is conducted. The simulation had a good agreement with the experimental results. The cost-effective, compact and powerful laser source opens up new possibilities for research and industrial applications.

Keywords: diode pump; GHz repetition rate; high power; Kerr-lens mode locking; solid-state laser

1. Introduction

Femtosecond lasers with gigahertz (GHz) repetition rate act as a cornerstone for the development of femtosecond optical frequency combs (OFCs), which are an indispensable tool for high-precision frequency metrology[1], fast spectroscopy with resolved comb lines[2], astronomical spectrometer calibration[3] and other applications requiring simple access to the individual comb lines. In recent years, dual-comb spectroscopy has drawn the interest of the scientific community due to the fast acquisition speed in spectroscopic applications[4]. However, the traditional dual combs usually require two fully stabilized OFCs with slightly different repetition rates, which makes the system complex. Currently, the development of single-cavity dual-comb lasers provides an emerging way to solve the problem, and has become a powerful tool for dual-comb spectroscopy[5–10]. Furthermore, dual combs with GHz spacing have the advantages of sufficient density of comb lines to directly observe absorption features, fast update rates and high sensitivity in signal measurements[11,12], leading to them recently being studied eagerly. However, it is challenging to obtain GHz mode-locked femtosecond lasers due to the relatively low intracavity pulse energy and the compact geometry.

To date, mode-locked femtosecond lasers with GHz repetition rates have been realized by various schemes, such as fundamental or harmonic mode-locked fiber lasers[13,14], mode-locked vertical external-cavity surface emitting lasers (VECSELs)[15], all-solid-state lasers (ASSLs) based on semiconductor saturable absorber mirrors (SESAMs)[16] and Kerr-lens mode locking[17]. Trade-offs are unavoidable

Correspondence to: W. Tian and J. Zhu, School of Optoelectronic Engineering, Xidian University, Xi'an 710071, China. Emails: wltian@xidian.edu.cn (W. Tian); jfzhu@xidian.edu.cn (J. Zhu)

for different applications according to the benefits. Among them, a polarization multiplexing VECSEL with the repetition rate of 10 GHz has been demonstrated for dual-comb spectroscopy measurements of water vapor[5]. Ten-GHz passively mode-locked ASSLs based on SESAMs have also been reported[16], and watt-level average power was achieved from a customized SESAM and a high-power multimode pump laser diode (LD). With Kerr-lens mode-locking technology, the highest repetition rate was up to 10 GHz in green laser pumped Ti:sapphire lasers[18] and 23.8 GHz in LD-pumped Yb-doped ASSLs[17]. However, the beam waist of the pump and the laser beam is tightly focused in GHz resonators, which requires an excellent pump beam quality ($M^2 \sim 1$) to form a soft aperture inside the gain medium[19], such as single-mode fiber-coupled LDs. As a result, the average output power of Yb-doped GHz Kerr-lens mode-locked (KLM) oscillators has been consequently restricted to the few tens of milliwatts range, which limits further applications. Recently, we have demonstrated watt-level average output power in Yb-doped GHz KLM oscillators for the first time by using a single-mode fiber laser as the pump source. Bidirectional mode-locked operation was also demonstrated, but the scaling of average power is still constrained by the limited pump power[20]. Another work showed that watt-level average power can be realized in multimode fiber-coupled LD-pumped Yb-doped GHz KLM oscillators as well[21]; the key is that a hard aperture was introduced for increasing the loss of the continuous wave (CW). It is suited for lasers with linear cavities and it is difficult to further increase the average power and repetition rate. In contrast, the bow-tie ring cavity based on the soft aperture effect is more appropriate for multi-GHz femtosecond laser generation with Kerr-lens mode locking, which also has the potential to be a single-cavity dual-comb source based on the directional dependence of the Kerr nonlinearity[10,22]. However, to the best of our knowledge, there are currently no reports on multimode LD-pumped GHz KLM lasers with a bow-tie ring cavity.

Here, we redesign the ring cavity so that it satisfies the requirement of soft aperture Kerr-lens mode locking when pumped by a multimode LD with a poor beam quality. The unique cavity geometry consists of two pairs of concave mirrors that produce two beam waists within the cavity. One of the waists is large enough to match well with a multimode fiber-coupled LD. The other small waist allows employing an additional Kerr medium to increase self-phase modulation (SPM) or using a nonlinear crystal to realize intracavity frequency conversion[23]. In order to realize Kerr-lens mode locking easily, we present a numerical simulation method that provides guidance to search for the mode-locking regime; the variation of stability and the strength of Kerr-lens mode locking are also characterized at different intracavity peak powers. As proof-of-principle experiments, unidirectional KLM operations with 3.3- and 6.13-W average powers as well as bidirectional KLM operation with average powers of 3.7 and 3.8 W, respectively, at the repetition rate of 1.6 GHz were obtained from a multimode LD-pumped KLM Yb:KGW oscillator. This approach opens up a new way to generate high-power GHz KLM lasers and the numerical simulation method provides guidance to achieve stable high-power KLM operation.

2. Experimental setup: design and simulation

2.1. Experimental design

A dual-confocal ring cavity was proposed as shown in Figures 1(a) and 1(b); the cavity consisted of two pairs of concave mirrors with radius of curvature (ROC) of 50 and 30 mm, respectively. Here, we set two configurations with different output couplers (OCs) and group delay dispersion (GDD). In the two configurations, one of the mirrors with ROC of 50 mm has transmittance of 1% and 2% as the OC. To compensate for the intracavity positive GDD and balance the nonlinearity, Gires–Tournois interferometer (GTI) mirrors were used to provide a negative GDD. For the first configuration with a 1% OC, approximately –1200 fs^2 GDD around 1035–1055 nm was provided by one of the mirrors with an ROC of 30 mm, and the other one was a dichroic mirror. For the second configuration with a 2% OC, the total GDD of –1100 fs^2 around 1020–1050 nm was provided with two concave mirrors of 30 mm ROC. Due to the dual-confocal geometry, two laser waists are formed in this resonator, as shown in Figures 1(c) and 1(d). In CW operation (blue curve), one of them has a radius of approximately 65 μm, which is slightly larger than that of the pump beam, and it shrinks to 55 μm in pulsed operation, which matches better with the pump beam; this behavior enables Kerr-lens mode locking based on the soft aperture effect to be implemented. The other one has a smaller radius of approximately 39 μm in CW operation and shrinks to approximately 33 μm in pulsed operation (orange curve), which is beneficial for employing an additional Kerr medium or conducting frequency doubling. It is therefore feasible to realize GHz Kerr-lens mode locking pumped by a multimode LD. In this proof-of-principle experiment, we did not employ an additional Kerr medium, instead using a 2-mm-long Yb(5%, atomic fraction):KGW crystal with a high nonlinear coefficient (2×10^{-15} cm^2/W), which acts as both the gain medium and the Kerr medium. The pump laser was a multimode fiber-coupled LD with 105-μm core diameter (BWT, $M^2 \approx 19.5$), which can offer a maximum pump power of 60 W at 980.5 nm. The pump beam was shaped through a commercially available coupling optics system that has an imaging ratio of 1:1 and a transmission of 97% for the pump wavelength. The focused pump spot size was measured to be about 101 μm × 104 μm ($1/e^2$).

https://doi.org/10.1017/hpl.2024.42 Published online by Cambridge University Press

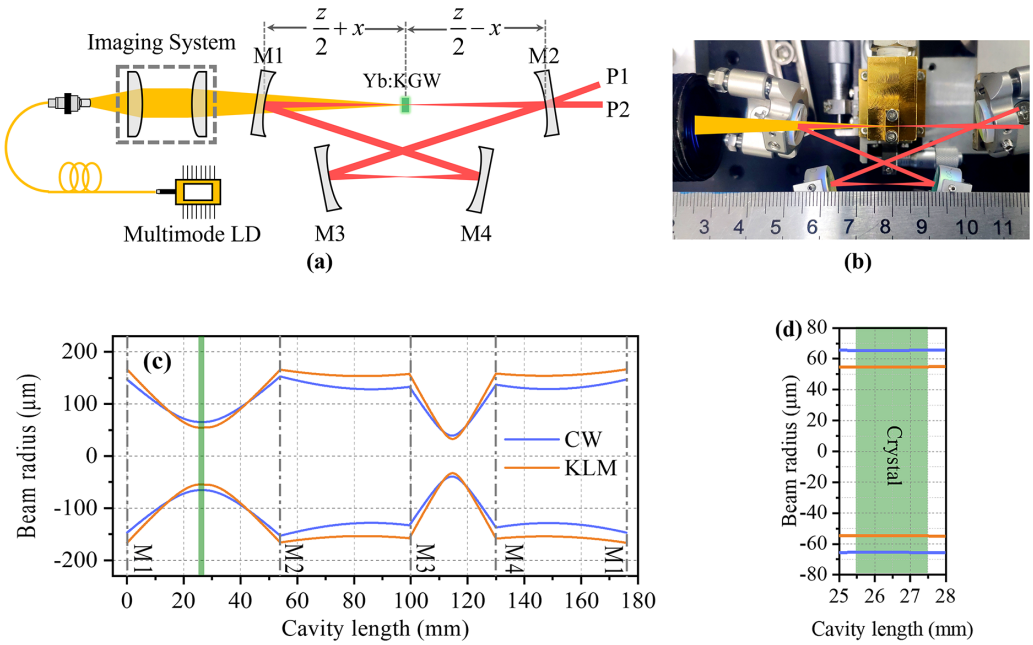

Figure 1. (a), (b) Schematic and corresponding photo of the dual-confocal Yb:KGW ring cavity. M1 and M2 have a radius of curvature (ROC) of 50 mm. M2 also acts as the OC with transmittance of 1% and 2% in two configurations. M3 and M4 have an ROC of 30 mm and provide the total GDD of –1200 and –1100 fs^2 in two different experiments. (c) Laser beam radius throughout the whole ring cavity, in which the green area marks the position of the gain crystal. (d) Detail of the beam radius inside the gain crystal.

2.2. Simulation method for Kerr-lens mode locking

For realizing Kerr-lens mode locking, the soft aperture effect is a prerequisite. In addition, the mode matching between the pump spot and the circulating laser is a key factor for realizing stable high-power KLM operation. Here we define the mode matching ratio η that is equal to the ratio of the pump waist to the laser waist in the crystal. This ratio η characterizes the loss of the pulsed laser. When the value of η is close to 1, that is, the beam sizes of the pump and the laser are approximately equal, the loss of the pulsed laser is minimized. As well as mode matching, the Kerr sensitivity parameter δ that describes the relative spot size variation is also considered significant. It is widely used to quantitatively evaluate the stability of KLM operation. The larger absolute value of δ indicates more stable mode locking and self-starting is possible, which is defined as follows[24]:

$$\delta = \frac{1}{\omega}\frac{\mathrm{d}\omega}{\mathrm{d}P}, \tag{1}$$

where ω is the mode radius at a given plane inside the resonator, which is a function of the intracavity peak power, P. In the case of small signal relative spot size variation ($P = 0$, CW operation), the calculation of the δ parameter is simple and it can provide the basic guidelines for searching the regime of Kerr-lens mode locking. However, both the beam sizes of the laser and the pump are reduced simultaneously as a result of the changed refractive index of the crystal caused by the self-focusing effect. In addition, the corresponding values of η and δ vary accordingly. Therefore, the calculation of η and δ at different stability regimes and at different intracavity peak powers is necessary when it comes to high-power KLM operation. For more accurate quantification of the high-power KLM operation, the normalized intracavity peak power is defined as follows:

$$K = P/P_{\mathrm{c}}, \tag{2}$$

where P_c is the critical intracavity power for self-focusing, which is related to the carrier wavelength λ, linear refractive index n_0 and the nonlinear coefficient n_2, defined as follows:

$$P_{\mathrm{c}} = \frac{\alpha\lambda^2}{4\pi n_0 n_2}, \tag{3}$$

where α is a constant calculated to be 1.86–2.0 for a Gaussian beam[25]. Using the normalized intracavity peak power K to evaluate the Kerr-lens mode locking operation, Equation (1) is extended as follows:

$$\delta_K = \frac{1}{\omega}\frac{\mathrm{d}\omega}{\mathrm{d}K}. \tag{4}$$

The case of $K = 0$ corresponds to Equation (1), which represents CW operation. According to Equation (4), the δ_K parameter can be calculated at different intracavity peak powers and the optimal intracavity peak power can be predicted. When it is negative, the mode radius would be reduced with the increase of intracavity peak power, which

https://doi.org/10.1017/hpl.2024.42 Published online by Cambridge University Press

indicates that self-focusing occurs due to the enhanced Kerr-lens effect so that the system can support KLM operation with a soft aperture. In 1993, Magni *et al.*[24] presented an analytical method to calculate the Kerr sensitivity of linear cavities, where the nonlinearity effect of the Kerr medium was approximated as a thin element with lumped Kerr nonlinearity. However, the analytical method is not easily applied to ring cavities and the thin element approximation of the Kerr effect is less precise for a thick Kerr medium due to the variation of laser mode sizes at different positions inside the thick Kerr medium. Xia *et al.*[26] quantified the Kerr sensitivity of ring cavities by calculating the self-consistent Gaussian mode based on the *ABCD* matrix, but the same approximation of Kerr nonlinearity was followed as by Magni *et al.*[24].

To quantify KLM operation more precisely, we optimized the above methods. The Kerr nonlinearity was regarded as a stack of nonlinear lenses whose focal length depends on the beam radius and laser intensity. For a Gaussian beam, the beam size $\omega_K(z)$ and ROC $R_K(z)$ can be described by the q parameter:

$$\frac{1}{q_K(z)} = \frac{1}{R_K(z)} - i\frac{\lambda}{\pi\omega_K{}^2(z)}. \tag{5}$$

Based on the *ABCD* matrix, $\omega_K(z)$ and $R_K(z)$ can be given by the following:

$$R_K(z) = \frac{2B}{D-A}, \tag{6}$$

$$\omega_K^2(z) = \frac{|B|\lambda}{\pi}\sqrt{\frac{1}{1-(A+D)^2/4}}, \tag{7}$$

where A, B, C and D are the elements of the cavity propagation matrix. In CW operation ($K = 0$), the solution of the q parameter is straightforward because the transformation of the Gaussian beam in the Kerr medium can be calculated by standard *ABCD* law. In contrast, the solution of the spatial mode in KLM operation ($K > 0$) is complicated. Due to the Kerr-lens effect, the cavity mode depends on the optical intensity, which, in return, depends on the cavity mode, leading to crosstalk between them. Here, the solution of the q parameter is calculated iteratively. A flowchart of the simulation is shown in Figure 2. Starting with the solution of q_{CW} ($K = 0$) as the initial iteration value, the *ABCD* matrix of the nonlinear Kerr lens can be calculated based on the beam radius in the crystal given by q_{CW}. Then a new matrix of the resonator including the Kerr effect is achieved, and the new solution of beam radius will be found. The iteration is continued in this manner until the q parameter is obtained at assumed intracavity peak power K. In this simulation approach, the calculation accuracy of the Kerr-lens effect directly affects the results of the q_K parameter. If the diopter of the Kerr lens is represented by a thin lens approximatively, non-negligible errors will be introduced when the thickness of the Kerr medium is larger than the Rayleigh range of the laser mode. For calculating the diopter of the Kerr-lens effect accurately, the Kerr-lens effect in the crystal is also

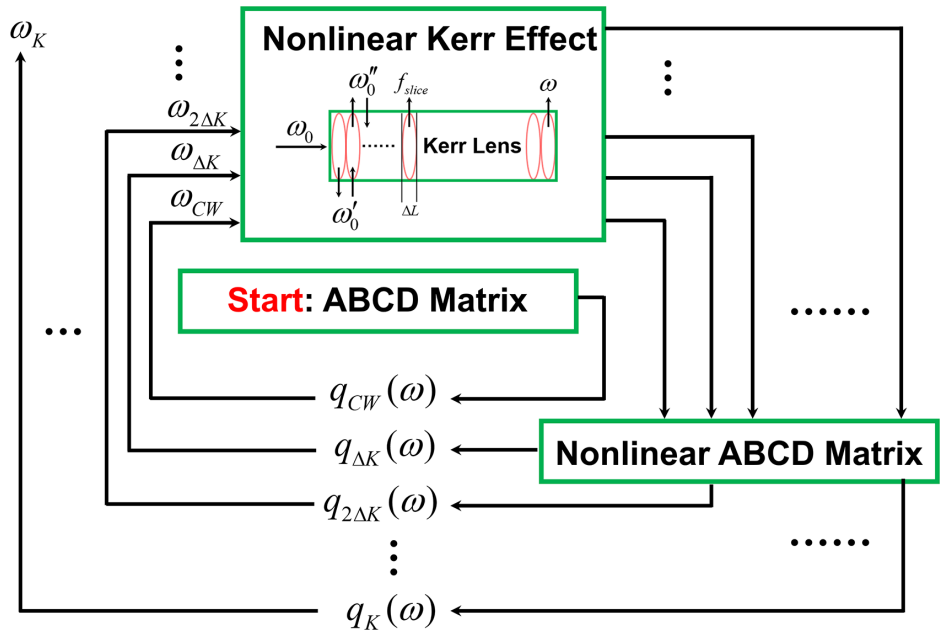

Figure 2. Flowchart of the simulation. The cavity mode is calculated by using q parameters, and the q parameters at different intracavity peak power K are calculated iteratively in steps of ΔK. In this way, we can obtain the cavity mode at any K according to Equation (7). In this process, the introduced nonlinear Kerr effect and the resonant cavity form the nonlinear *ABCD* matrix, where the calculation of the Kerr effect in the crystal is not equated to a thin lens. The laser crystal is split into a series of slices with a thickness of ΔL that is much less than the Rayleigh range, and the laser beam size in the crystal is calculated in an iterative manner, which avoids the coupling of the laser intensity and laser mode in the crystal.

https://doi.org/10.1017/hpl.2024.42 Published online by Cambridge University Press

calculated iteratively, as shown in Figure 2. The laser crystal is split into a series of slices with a thickness of ΔL that is much less than the Rayleigh range; then the nonlinear *ABCD* matrix of the crystal is represented by a stacking of each thin-lens matrix M_{slice}, which can be expressed as a nonlinear matrix and the propagation in a linear medium of length ΔL:

$$M_{\text{slice}} = \begin{bmatrix} 1 & 0 \\ -1/f_{\text{slice}} & 1 \end{bmatrix} \begin{bmatrix} 1 & \Delta L \\ 0 & 1 \end{bmatrix} = \begin{bmatrix} 1 & \Delta L \\ -1/f_{\text{slice}} & 1 \end{bmatrix}. \tag{8}$$

In Equation (8), f_{slice} is the equivalent focal length of each slice caused by the Kerr-lens effect. The self-focusing effect of the Gaussian beam propagating in a medium is related to the intensity-dependent nonlinear refractive index n_2, which can be described by a radially varying refractive index $n(r)$. In an aberration-free system, $n(r)$ is given by the following:

$$n(r) = n_0 + n_2 I_0 \mathrm{e}^{-2r^2/\omega^2}, \tag{9}$$

where n_0 is the linear index of refraction and I_0 is the laser peak intensity. The optical path difference (OPD) in the crystal is generated due to the refractive index difference between the center and the radial direction of the slice, which can be expressed as follows:

$$\mathrm{OPD}(r) = \Delta L[n(0) - n(r)] = \Delta L n_2 I_0 \left(1 - \mathrm{e}^{-2r^2/\omega^2}\right). \tag{10}$$

According to the geometric properties of the Gaussian beam focusing, the OPD can also be described by $n_0\left[\sqrt{r^2 + f^2(r)} - f(r)\right]$, and it can be approximated as $n_0 r^2/2f(r)$ by neglecting the higher order terms that have omitted in the expansion due to the much smaller r than $f(r)$. As a result, in Equation (10) the equivalent focal length $f(r)$ of a slice as a function of r can be rewritten:

$$f(r) = \frac{n_0 r^2}{2\Delta L n_2 I_0 \left(1 - \mathrm{e}^{-2r^2/\omega^2}\right)}. \tag{11}$$

The center of laser beam ($r = 0$) has the strongest focusing power:

$$f_{\text{center}} = f(0) = \frac{n_0 \omega^2}{4\Delta L n_2 I_0}. \tag{12}$$

It is not reasonable to use f_{center} directly to represent the equivalent focal length f_{slice} because of the radially varying focusing strength. Therefore, the weighted average focal length f_{av} is calculated to characterize f_{slice}, defined as follows:

$$f_{\text{av}} = \frac{\int_0^{+\infty} I(r) \cdot 2\pi r \cdot f(r) \mathrm{d}r}{\int_0^{+\infty} I(r) \cdot 2\pi r \mathrm{d}r} \approx 1.645 \frac{n_0 \omega^2}{4\Delta L n_2 I_0}. \tag{13}$$

Combining the weighted average focal length of Equation (13) and the thin-lens matrix M_{slice}, one can calculate the nonlinear Kerr-lens effect in the laser crystal. By the iterative calculations of the q_K parameter and the nonlinear *ABCD* matrix, the cavity modes and the δ_K parameter can be obtained at arbitrary intracavity peak power K. The evolution of the pump waist can also be simulated by the q_K parameter based on Gaussian beam propagation, where we approximate that the Kerr effect on the pump laser is the same as the circulating laser. As a result, the mode matching ratio η can be simulated. According to the calculations of η and δ_K, the optimal regime and intracavity peak power can be predicted.

3. Results and discussion

3.1. Predictions of the KLM regime

We firstly calculated the relative spot size variation δ_K at $K = 0$, as shown in Figure 3(a), where z is the distance between the concave mirrors on both sides of the Yb:KGW crystal and x is the displacement between the laser waist and the center position of the crystal (see Figure 1(a)). The self-consistent solutions are in the colored region; the closer to the edge of the inner stability, the larger $|\delta_K|$ is, indicating that the Kerr-lens mode locking can be initiated more easily. The small displacement x had a negligible effect on δ_K. Based on the guidance, one can search for the mode-locking regime toward the inner stability. For the high-power operation, the parameter was calculated at $K = 1$, 1.5 and 2 to facilitate the search for positions of Kerr-lens mode locking. In contrast to the CW operation, the regime of the stability map decreases with the increase of intracavity peak power, indicating that the stable CW operation will evolve to unstable pulse propagation in this range during the KLM process, as depicted in Figures 3(b)–3(d). At $K = 1$, the maximum of δ_K is close to the edge around $z = 52$ mm of inner stability. When K increases, the regime of the maximal δ_K gradually moves in the direction of increasing z. For example, the maximal δ_K exists around 52.9 mm $< z <$ 53.6 mm at $K = 1.5$, and 53.8 mm $< z <$ 55.3 mm at $K = 2$, where stable Kerr-lens mode locking is relatively easy to realize. In addition, the stable pulse operation also depends on the balance of gain and loss in the cavity, as well as being sensitive to the intracavity power. Proper intracavity peak power is important for the formation of soliton pulses. Consequently, we further calculated the variation of the δ_K parameter and the mode matching ratio η as a function of intracavity peak power K for some fixed configurations ($z = 53$, 53.5, 54 and 54.5 mm), as shown in Figures 3(e) and 3(f); there are always inflection points, and their values vary with different distance of z. The absence of partial solutions in the curves indicates that the cavity is unstable in this case.

https://doi.org/10.1017/hpl.2024.42 Published online by Cambridge University Press

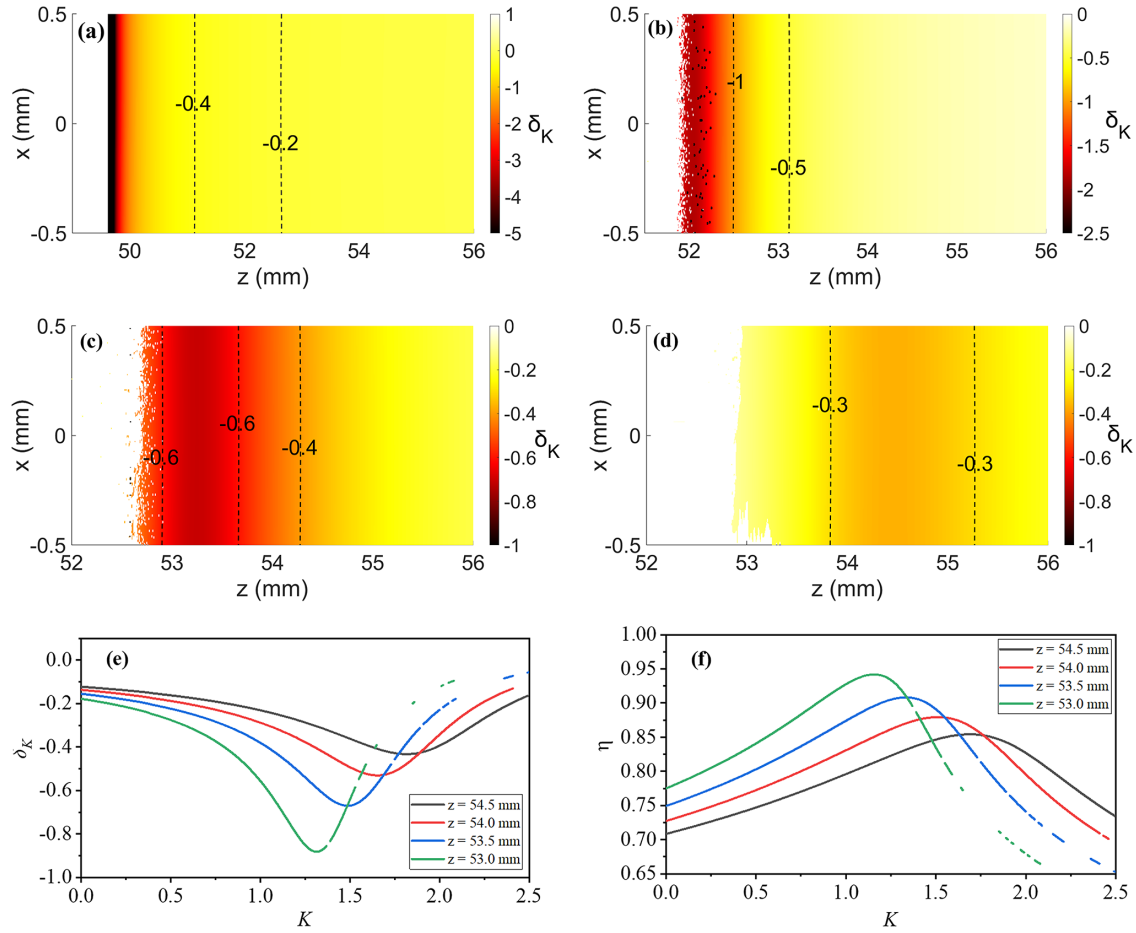

Figure 3. (a)–(d) The stability maps are simulated at various normalized intracavity peak powers of $K = 0$, 1, 1.5 and 2. Here, z is the distance between the concave mirrors on both sides of the crystal, and x is the displacement between the laser waist and the center position of the crystal (see Figure 1(a)). The absolute value of δ_K increases gradually when it is closer to the edge of the inner stability at $K = 0$. However, at $K = 1$, 1.5 and 2, δ_K always maintains a large value within a certain regime, which offers us a direction in our quest for the KLM regime. (e), (f) Variation of the δ_K parameter and the mode matching ratio η with the intracavity peak power K for some fixed configurations, indicating that the best intracavity peak power varies with z; the various configurations have different optimal values of δ_K and η, leading to a different K.

The simulated curves describe the dynamic of the Kerr-lens mode locking. Origin pulses are generated by optimizing the CW operation close to the edge of inner stability, accompanied by an increase of the intracavity peak power K and an enhanced self-focusing effect. As a result, the beam radius inside the crystal reduces so that $|\delta_K|$ becomes larger and the mode matching ratio η increases, which means that the loss of pulsed laser reduces. When η reaches the extremum value, the pulsed laser gets the maximal gain while the CW laser gets the maximal loss. In this instance, soft aperture Kerr-lens mode locking and the stable pulse operation are easy to establish. If one only considers the influence of η for stable KLM operation, as shown in Figure 3(f), the optimal K should be slightly larger than the value at the inflection point, where the mode matching ratio η will deteriorate as K continues to increase and cause a reduction in the average power. The reduced average power in turn causes a lower value of K, leading to a larger laser mode and better mode matching. Consequently, it will play a balancing role and keep the mode locking stable when K is fluctuating. On the other hand, the larger $|\delta_K|$ is, the easier it is to initialize and maintain stable Kerr-lens mode locking. So in order to obtain a stable high-power KLM operation, one should take into account the influence of η and $|\delta_K|$. It is worth noting that the maxima of η and $|\delta_K|$ correspond to an almost equal value of K at a fixed z, as shown in Figures 3(e) and 3(f), which indicates that it is preferable to achieve stable Kerr-lens mode locking with the configuration where K is larger than the maximum η and around the inflection point of $|\delta_K|$. As further illustrated in Figure 3(e), the smaller z is, that is, the closer to the edge of the inner stability, the larger the $|\delta_K|$ value and the better mode matching that may be attained, while a smaller corresponding K at the inflection point indicates that the power supported during steady-state mode locking is lower. In a trade-off between them, the ideal condition of z for achieving high power is between 53.5 and 54 mm for this cavity.

https://doi.org/10.1017/hpl.2024.42 Published online by Cambridge University Press

3.2. Mode-locking results

The implementation of Kerr-lens mode locking is guided by the simulation. At first, the mirror M2 with 1% transmission was used as the OC. According to the simulation, the CW operation was firstly optimized around $z \approx 53.5$ mm, and the self-starting Kerr-lens mode-locking operation occurred at 22.3-W pump power by finely adjusting to $z \approx 53.8$ mm, which has a good agreement with the predicted regime of $z = 53.5$–54 mm. The output power of P2 grew to 3.3 W once the Kerr-lens mode locking was initiated, while the output power of P1 dropped to 0.6 W. Using an optical spectrum analyzer and an intensity auto-correlator, the optical spectrum and temporal features were subsequently assessed. The optical spectrum of the pulses was centered at 1049 nm, with a full-width at half-maximum (FWHM) bandwidth of 5 nm (Figure 4(a)). The measured intensity autocorrelation trace had an FWHM duration of 415 fs. Assuming a sech^2 pulse shape, the corresponding pulse duration was 269 fs (Figure 4(b)). Figure 4(c) shows the radio frequency (RF) spectra measured via a fast photodetector (bandwidth: 12.5 GHz) and an RF spectrum analyzer. The short-term stability of the mode-locked operation is proven by the RF spectrum. The fundamental signal had a distinct signal-to-noise ratio (SNR) of 57 dB beating at 1.64 GHz with a resolution bandwidth (RBW) of 10 kHz; the inset displays RF spectra of the pulse trains in the 10 GHz region, where there is no significant spectral modulation.

The 3.3-W average power with 269-fs pulse duration was realized at repetition rate of 1.64 GHz, corresponding to a peak power of 6.58 kW ($P_{peak} = S_p P_{av}/(f_{rep}\tau)$, where S_p is the pulse shape factor, $S_p = 0.88$ for sech^2 pulses). With 1% transmittance of the OC, the intracavity peak power was 658 kW, resulting in a normalized intracavity peak power $K = 1.57$ ($P_c = 418.5$ kW). In this case, we calculated the η and $|\delta_K|$ as a function of K at $z = 53.8$ mm, and the maxima of η and $|\delta_K|$ are 0.890 and –0.580 at $K = 1.45$ and $K = 1.59$, respectively, as shown in Figures 5(a) and 5(b). The experimental intracavity peak power K of 1.57 is very close to the simulation value for the maximal $|\delta_K|$ and is slightly larger than the simulation value for the maximum η, which has a good agreement with the simulations.

To obtain higher average power, the OC was replaced with a larger transmittance of 2%. As shown in Figure 3(e), it is worth noting that if the intracavity peak power K is increased further, the absolute value of $|\delta_K|$ at the inflection point would decrease, making it difficult to initiate Kerr-lens mode locking. By slightly reducing the length of both arms, it was found that the resonant cavity can handle more power while keeping an acceptable $|\delta_K|$ value. Thus, the length of

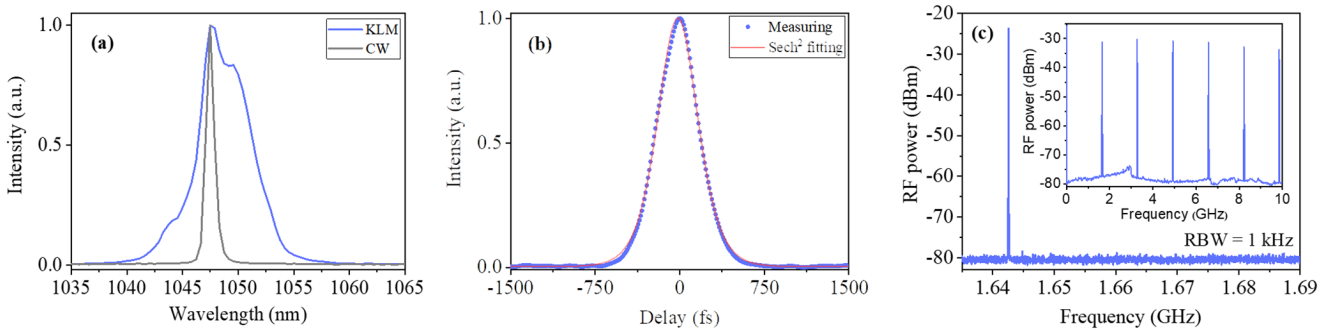

Figure 4. Mode-locking characterization of the 1.64-GHz dual-confocal ring Yb:KGW oscillator with a 1% OC. (a) Optical spectrum of the mode-locked pulses centered at 1049 nm, with a full-width at half-maximum (FWHM) bandwidth of 5 nm. (b) Intensity autocorrelation trace with sech^2-fitting of 269 fs indicated by the red curve and measured data with blue dots. Inset, autocorrelation trace measured in a 50 ps delay span. (c) Radio frequency spectrum of the fundamental repetition at 1.64 GHz and the harmonics within a 10 GHz span at 10 kHz RBW.

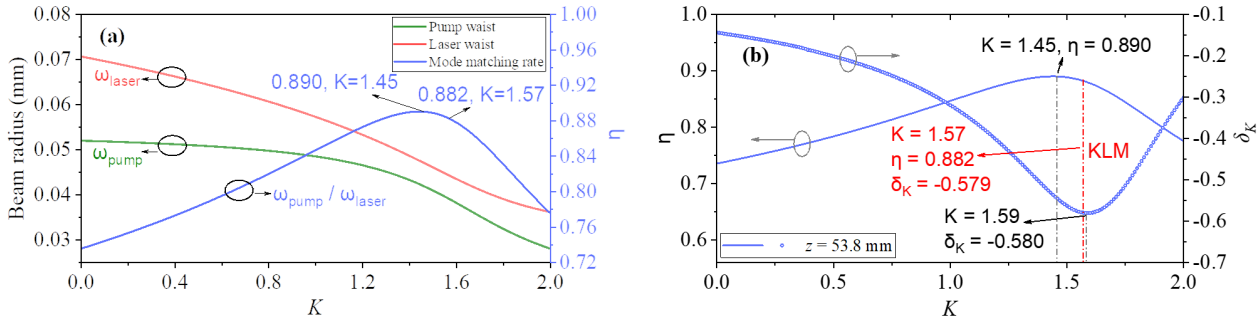

Figure 5. Simulations of the 1.64-GHz dual-confocal ring Yb:KGW oscillator with a 1% OC. (a) The variation with the intracavity peak power K of the pump waist, laser waist and the mode matching ratio η at the position of Kerr-lens mode locking. (b) The variation of η and the $|\delta_K|$ parameter with the intracavity peak power K at the position of Kerr-lens mode locking.

https://doi.org/10.1017/hpl.2024.42 Published online by Cambridge University Press

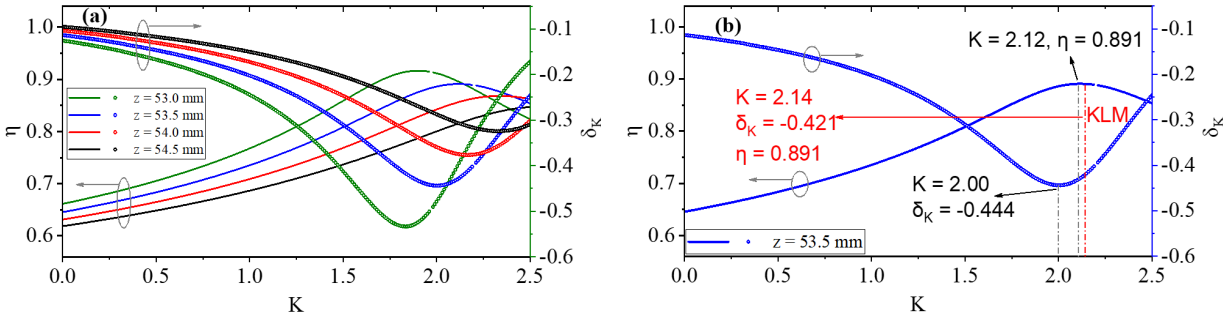

Figure 6. Simulations of the 1.68-GHz dual-confocal ring Yb:KGW oscillator with a 2% OC. (a) The parameters η and δ_K as a function of the intracavity peak power K for four fixed configurations. (b) The variation of η and the δ_K parameter with the intracavity peak power K at the position of Kerr-lens mode locking.

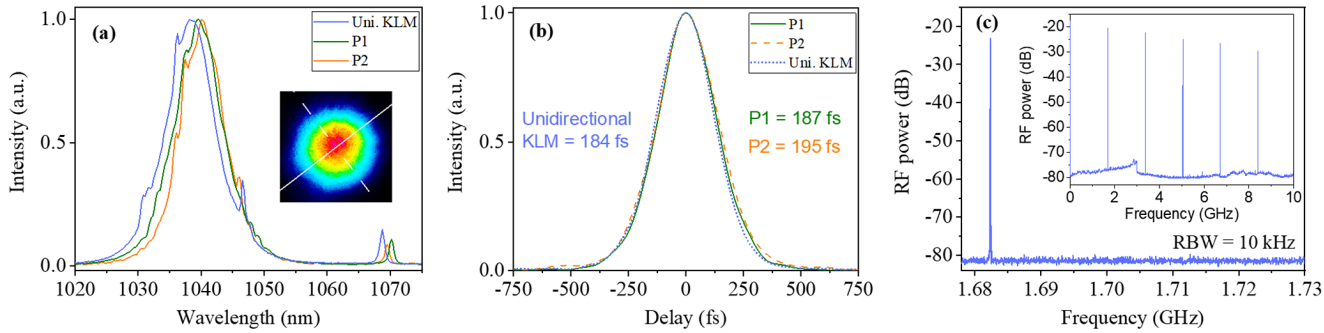

Figure 7. Mode-locking characterization of the 1.68-GHz dual-confocal ring Yb:KGW oscillator with a 2% OC. (a) The optical spectrum of bidirectional and unidirectional Kerr-lens mode locking, where the inset is the near-field beam profile of unidirectional KLM operation. (b) Intensity autocorrelation trace with sech^2-fitting of bidirectional and unidirectional KLM operation. (c) Radio frequency spectrum of the fundamental repetition at 1.68 GHz and the harmonics within a 10 GHz span at 10 kHz RBW.

the cavity was slightly reduced, and the design of the heat sink was modified to prevent crystal damage, including stress relief and heat dissipation. Using the same methods, the η and $|\delta_K|$ of this configuration were simulated, as shown in Figure 6(a). In high-power operation, such as $K > 2$, the predicted z needs to be greater than 53.5 mm (the blue curve in Figure 6(a)).

According to the guidance, the laser was firstly optimized in CW operation. The average output power of the bidirectional laser was 4.17 and 4.27 W in CW operation at the pump power of 30 W, and the optical-to-optical efficiency climbed to 28.1%. By finely adjusting the cavity alignment and the distance of z, bidirectional Kerr-lens mode locking was realized with average powers of 3. 7 and 3.8 W at 31.4-W pump power. The green and orange curves in Figure 7(a) show the optical spectra of bidirectional Kerr-lens mode locking, centered at 1039 and 1040 nm with respective FWHMs of 9 and 8 nm. Single transverse mode oscillation was obtained in both CW and KLM operation with the multimode pump LD, as illustrated in the inset of Figure 7(a). The measured pulse durations were 187 and 195 fs, as shown in Figure 7(b). The repetition rate is 1.68 GHz due to the slightly shortened cavity, as shown in Figure 7(c).

Unidirectional Kerr-lens mode locking is also demonstrated, in which case the mode-locked laser had an average power of 6.17 W and the other laser's power dropped to 0.9 W. The measured optical spectrum is centered at 1038 nm with an FWHM of 9 nm and the corresponding pulse duration was 184 fs, as also shown in Figures 7(a) and 7(b). The result of unidirectional Kerr-lens mode locking was obtained at $z = 53.5$ mm, with the parameter calculated of η and δ_K as shown in Figure 6(b). The maximum values of η and δ_K are 0.891 and –0.444, corresponding to the K values of 2.12 and 2.00, respectively. In this experiment, the normalized intracavity peak power K is 2.14 ($P_c = 409.8$ kW for this configuration), as marked by the red dotted line in Figure 6(b), and the corresponding η and δ_K are 0.891 and –0.421, respectively, which also match well with the predictions.

4. Conclusion

In conclusion, by designing the dual-confocal ring cavity, we overcome the issues faced by conventional GHz KLM oscillators in which the average power is limited to few tens of milliwatts. Two laser waists are formed in such geometry, one of which can mode-match well with the multimode fiber-coupled LD pump laser so that high-power KLM GHz oscillators are realized, which offers powerful sources for

https://doi.org/10.1017/hpl.2024.42 Published online by Cambridge University Press

compact OFC generation. The ring cavity geometry also has the potential to produce single-cavity dual-comb lasers that take advantage of the bidirectional Kerr-lens mode locking. Due to the sensitivity of KLM oscillators to cavity configuration and intracavity power, especially in the dual-confocal cavity, it is challenging to initiate Kerr-lens mode locking rapidly. We have proposed a numerical analysis method to predict the mode-locking regime, in which an accurate model for calculating the Kerr nonlinearity δ_K is employed in the self-consistent equation-based *ABCD* matrix. The values of η and the δ_K parameter as a function of normalized intracavity peak power K at different z allow us to determine where the stable Kerr-lens mode locking can be obtained. Combining the dual-confocal design and the numerical analysis method, we have demonstrated a multimode fiber-coupled LD-pumped KLM Yb:KGW oscillator around 1.6 GHz repetition rate, in which both high-power unidirectional and bidirectional Kerr-lens mode lockings were obtained. Higher average power and shorter pulse duration are expected by using OCs with high transmittance and a gain medium with a broad emission band. The attenuated Kerr nonlinearity caused by large OCs can be compensated by an additional Kerr medium positioned at the smaller waist in the dual-confocal cavity, which can enhance the SPM effect and enable the use of various laser crystals as gain media, even in the absence of a sufficiently high nonlinear coefficient. Not only is the cavity design applicable for the average power and pulse length scales, but also for the repetition rate scale. A higher repetition rate can be designed by employing the combinations of concave mirrors with smaller ROCs, and the cavity mode can also match well with a multimode LD and is appropriate for soft aperture Kerr-lens mode locking. The cavity design holds not just for ultrafast 1-μm laser sources, but it can also be deployed at other wavelengths, such as for GHz Cr:ZnS/ZnSe oscillators at longer wavelength in the mid-infrared band, because the GDD introduced by Cr:ZnS/ZnSe crystals can be compensated by the additional Kerr medium in the cavity, such as yttrium aluminum garnet (YAG), which has a negative GDD around 2 μm[27]. The new class of ultrafast lasers enabled by this technique represents an important step towards compact GHz KLM oscillators with tens of watt-level average power. These powerful sources will be desirable for applications involving high-power OFCs and dual-comb spectroscopy.

Acknowledgements

This work was supported by the National Key Research and Development Program of China (No. 2022YFA1604202), National Natural Science Foundation of China (No. 62105253), Natural Science Foundation of Shaanxi Province, China (No. 2023-JC-YB-485) and Shaanxi University of Technology (No. SLGRC202419). The numerical calculations in this paper were supported by the High-Performance Computing Platform of Xidian University.

References

1. T. Udem, R. Holzwarth, and T. W. Hänsch, Nature **416**, 6877 (2002).
2. S. A. Diddams, L. Hollberg, and V. Mbele, Nature **445**, 7128 (2007).
3. T. Steinmetz, T. Wilken, C. Araujo-Hauck, R. Holzwarth, T. W. Hänsch, L. Pasquini, A. Manescau, S. D'Odorico, M. T. Murphy, and T. Kentischer, Science **321**, 5894 (2008).
4. A. Bartels, R. Cerna, C. Kistner, A. Thoma, F. Hudert, C. Janke, and T. Dekorsy, Rev. Sci. Instrum. **78**, 035107 (2007).
5. S. M. Link, D. Maas, D. Waldburger, and U. Keller, Science **356**, 6343 (2017).
6. M. Kowalczyk, Ł. Sterczewski, X. Zhang, V. Petrov, Z. Wang, and J. Sotor, Laser Photonics Rev. **15**, 2000441 (2021).
7. J. Pupeikis, B. Willenberg, S. L. Camenzind, A. Benayad, P. Camy, C. R. Phillips, and U. Keller, Optica **9**, 713 (2022).
8. K. Fritsch, T. Hofer, J. Brons, M. Iandulskii, K. F. Mak, Z. J. Chen, N. Picqué, and O. Pronin, Nat. Commun. **13**, 2584 (2022).
9. S. Mehravar, R. A. Norwood, N. Peyghambarian, and K. Kieu, Appl. Phys. Lett. **108**, 231104 (2016).
10. T. Ideguchi, T. Nakamura, Y. Kobayashi, and K. Goda, Optica **3**, 748 (2016).
11. N. Hoghooghi, S. D. Xing, P. Chang, D. Lesko, A. Lind, G. Rieker, and S. Diddams, Light Sci. Appl. **11**, 264 (2022).
12. T. Voumard, J. Darvill, T. Wildi, M. Ludwig, C. Mohr, I. Hartl, and T. Herr, Opt. Lett. **47**, 1379 (2022).
13. A. Martinez and S. Yamashita, Appl. Phys. Lett. **101**, 041118 (2012).
14. A. Martinez and S. Yamashita, Opt. Express **19**, 6155 (2011).
15. B. W. Tilma, M. Mangold, C. A. Zaugg, S. M. Link, D. Waldburger, A. Klenner, A. S. Mayer, E. Gini, M. Golling and U. Keller, Light Sci. Appl. **4**, e310 (2015).
16. A. S. Mayer, C. R. Phillips, and U. Keller, Nat. Commun. **8**, 1673 (2017).
17. S. Kimura, S. Tani, and Y. Kobayashi, Optica **6**, 532 (2019).
18. A. Bartels, D. Heinecke, and S. A. Diddams, Science **326**, 5953 (2009).
19. S. Yefet and A. Pe'er, Appl. Sci. **3**, 694 (2013).
20. L. Zheng, W. L. Tian, H. Liu, G. Y. Wang, C. Bai, R. Xu, D. C. Zhang, H. N. Han, J. F. Zhu, and Z. Y. Wei, Opt. Express **29**, 12950 (2021).
21. M. Hamrouni, F. Labaye, N. Modsching, V. J. Wittwer, and T. Südmeyer, Opt. Express **30**, 30012 (2022).
22. I. Coddington, N. Newbury, and W. Swann, Optica **3**, 414 (2016).
23. J. Zhang, M. Pötzlberger, Q. Wang, J. Brons, M. Seidel, D. Bauer, D. Sutter, V. Pervak, A. Apolonski, K. F. Mak, V. Kalashnikov, Z. Y. Wei, F. Krausz, and O. Pronin, Ultrafast Sci. 2022, 9837892 (**2022**).
24. V. Magni, G. Cerullo, and S. D. Silvestri, Opt. Commun. **101**, 365 (1993).
25. G. Fibich and A. L. Gaeta, Opt. Lett. **25**, 335 (2000).
26. P. Y. Xia, M. Kuwata-Gonokami, and K. Yoshioka, Jpn. J. Appl. Phys. **59**, 062002 (2020).
27. A. Barh, B. Ö. Alaydin, J. Heidrich, M. Gaulke, M. Golling, C. R. Phillips, and U. Keller, Opt. Express **30**, 5019 (2022).

https://doi.org/10.1017/hpl.2024.42 Published online by Cambridge University Press